Mater.Phys.Mech.1 (2000) 39-44

CORRELATION BETWEEN SUPERCONDUCTING TRANSPORT PROPERTIES AND GRAIN BOUNDARY MICROSTRUCTURE IN HIGH-T_C SUPERCONDUCTING CERAMICS

T.S. Orlova[1], J.Y. Laval[2] and B.I. Smirnov[1]

[1]A.F. Ioffe Physico-Technical Institute, Russian Academy of Sciences, Polytechnicheskaya 26, 194021 St.Petersburg, Russia,
[2]Laboratoire de Physique du Solide, CNRS ESPCI, 10 rue Vauquelin, 75231 Paris Cedex 05, France

Received: October 21, 1999

Abstract. The superconducting transport properties (*I–V, I_c–B* and *I_c–T*) were correlated with a systematic characterization of the grain boundary microstructure, via TEM observation and local chemical analysis in STEM by EDX on $YBa_2Cu_{3-x}O_y$ (D samples), $YBa_2Cu_{3-x}O_y/Ag_x$ (S samples) and $DyBa_2Cu_{3-x}O_y$/1wt% Pt ($0 \le x \le 0.4$) ceramics. It was shown that in all samples studied the critical current I_c is controlled by weak links at grain boundaries. The measurements of $I_c(T)$ indicated that in copper-deficient yttrium ceramics, Ag-doping leads to change of weak link character from superconductor-insulator-superconductor (SIS) to superconductor-normal metal-superconductor (SNS) type. This SNS behaviour seems to be a result of percolation path of supercurrent through clean boundaries with extremely narrow range ($\cong$1 nm) of Ag segregation on them. Specific Ag precipitates of 2-5 nm size on or near clean boundaries were found in S samples for x=0.4. This is most likely to be a reason for the improvement of I_c in these samples by a factor of 3. In copper-deficient dysprosium ceramics doped with Pt, Pt-doping leads to a substantial increase in I_c and pronounced 'fish-tail' effect in magnetic field at $T \le 77$ K in non-stoichiometric composition with x=0.2. Better behaviour of I_c in magnetic fields in these samples may be associated with the substantial increase in the proportion of clean boundaries and decrease in twin spacing.

1. INTRODUCTION

In the high-T_c granular superconductors, transport properties are mainly controlled by the grain boundary microstructure unlike T_c which is determined by the crystal structure and oxygen content. Depending on crystallography and structure of boundaries, they can be favourable for the passage of supercurrent or can be weak links (reduced I_c regions) in the superconducting current path of a ceramic sample. Recently many studies have been directed at investigating the dissipation at a separate boundary of different type [1]. Although studies of separate boundary behaviour highly contribute to understanding transport in superconducting polycrystalline materials, they are rather idealistic models of true polycrystalline materials which contain many boundaries of different types, in parallel and series, simultaneously. So, along with the study of a separate boundary, it is also very important to investigate the relation between transport properties and grain boundary behaviour as a network of boundaries.

The main aim of this work was to find possible correlation between microstructure features and superconducting transport properties. One way for changing intergrain critical current density of polycrystalline materials is doping with different elements. Small deviation from the stoichiometric composition can also lead to a change in structure and distribution of boundaries in a ceramic sample.

So, in this work the superconducting transport properties (*I–V*, *I_c–B* and *I_c–T*) were correlated with a systematic characterization of the grain boundary microstructure, via TEM observation and local chemical analysis in STEM by EDX. The following superconducting ceramics were studied.

1. $YBa_2Cu_{3-x}O_y$ ($0 \le x \le 0.4$) – Cu-deficient yttrium ceramics (D samples); $YBa_2Cu_{3-x}O_y/Ag_x$ ($0 \le x \le 0.4$) ceramics with silver incorporated in amounts equal to the copper deficiency (S samples).
2. $DyBa_2Cu_{3-x}O_y$/1wt% Pt ($0 \le x \le 0.4$) – Cu-deficient dysprosium ceramics doped with 1 wt% Pt.

Corresponding author: T.S. Orlova; e-mail: orlova.t@pop.ioffe.rssi.ru

2. EXPERIMENTAL

The YBCO ceramic system was fabricated via the modified citrate gel process [2]. The sol-gel method allows one to achieve highly homogeneous mixing of cations on an atomic scale and produce high-quality powder. Two types of YBCO samples were prepared. In samples of the first type $YBa_2Cu_{3-x}O_y$ ($0 \le x \le 0.4$) (D type) Cu-deficient compositions were obtained. In samples of the second type, $YBa_2Cu_{3-x}O_y/Ag_x$ ($0 \le x \le 0.4$) (substituted S type), Ag was considered as a substituent for Cu.

The copper deficient ceramics, $DyBa_2Cu_{3-x}O_y$, doped by 1wt.% Pt, were prepared by the usual solid state reaction. For comparison two compositions with x=0 and x=0.2 of the copper deficient ceramics $DyBa_2Cu_{3-x}O_y$ without Pt were also fabricated using the same method.

The phase were characterised by powder X-ray diffraction (XRD) using a Philips automated X-ray diffractometer. Microstructure and chemical compositions were analysed with a Jeol 2000 FX TEM equipped with a Link EXL X-ray selective analyser and with an SEM equipped with an EDAX X-ray selective analyser.

The superconducting properties were studied by measuring the resistivity-temperature (R–T) and current-voltage (I–V) characteristics using the four-probe technique. The critical current I_c was determined at various temperatures using the 1 $\mu V \cdot mm^{-1}$ criterion, with and without external magnetic field B. The external magnetic field ranged from 0 to 75 G and was perpendicular to the transport current.

3. RESULTS AND DISCUSSION

3.1 COPPER DEFICIENT YTTRIUM SYSTEM WITH AND WITHOUT AG-DOPING

First we will consider 123-yttrium system with copper deficiency with and without Ag-doping. According to the data in the literature [3-5] distribution of Ag in ceramics and its influence on J_c are subject to contradictory conclusions and strongly depend on composition of ceramics, processing technology and thermal treatment. Our ceramic samples were prepared via the modified citrate gel process [2] which allows one to achieve highly homogeneous mixing of cations on an atomic scale and produce high-quality homogeneous ceramics.

EDX analysis in TEM showed (Table 1) that the Ag content (x) of YBCO grains was lower than the nominal amount of Ag, in spite of the sol-gel method. Ag mainly precipitated as small particles (1–2 μm) homogeneously scattered throughout the sample.

Table 1. Average concentration of silver in the grains measured by EDX in TEM and STEM for $YBa_2Cu_{3-x}O_y/Ag_x$ for all doping levels.

Nominal Ag concentration x	*Real Ag concentration*
0.1	< limit of detection
0.2	≤0.02
0.4	0.03

X-ray diffraction and SEM analysis showed that all samples had an good orthorhombic structure. For samples with $x \ge 0.2$, along with Ag phase (S samples) several nonsuperconducting phases such as Y_2BaCuO_5 (211), $BaCuO_2$ (011) and CuO (D and S samples) were registrated. The amount of these nonsuperconducting phases (in D and S samples) and Ag-phase (S samples) increased with increasing x. Second phases such as $BaCuO_2$ and CuO were mainly located at grain boundaries and triple junctions. These impurity phases were about 1-3 μm in size, the mean distance between them was comparable with respective grain size. The average grain size dramatically decreased with x (Fig. 1). The nonsuperconducting phases and Ag precipitates appear to stop grain growth during sintering resulting in fine-grain microstructure for $x \ge 0.2$.

For all samples of both type (D and S) the critical temperature was practically the same (T_c=91-92 K), but the transport properties were quite different. Fig. 2 shows the measured values of critical current density J_c at 77 K versus x. For S samples, J_c increased only slightly with increase in Ag content from x=0 to x=0.2, whereas J_c increased more than threefold (from J_c=50 A/cm^2 for x=0 to J_c=170 A/cm^2) for x=0.4. For D samples with $x \ge 0.2$, J_c is ≅ twice that obtained for the stoichiometric composition.

It should be specially noted that in samples of both type (D and S), the obtained I–V curves at 77 K exhibited a power-low behaviour. I_c was strongly depressed

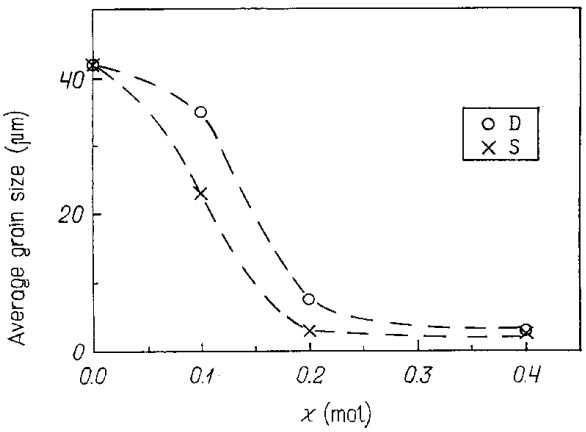

Fig. 1. Dependence of the average grain size of $YBa_2Cu_{3-x}O_y$ (D) and $YBa_2Cu_{3-x}O_y/Ag_x$ (S) samples on x.

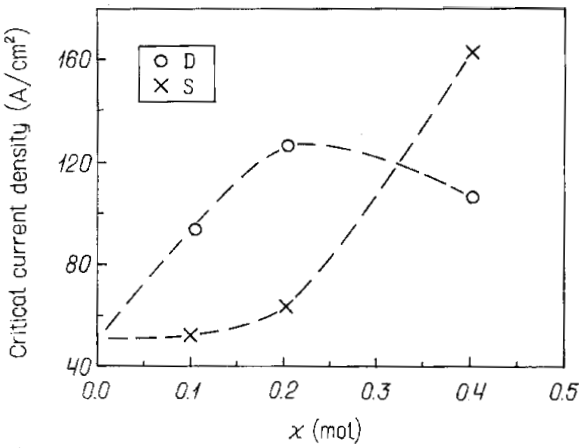

Fig. 2. Variation of the critical current with x for D and S samples.

by low magnetic fields. Such behaviour is characteristic of granular materials which can be described as a collection of superconducting grains connected by weak links [6].

Thus, in all samples I_c was controlled by grain boundary weak links which were characterized from $I_c(T)$ curves. It is known that for a Josephson tunnel (SIS) junction the dependence of I_c on temperature agrees with the equation I_c=const $(1\text{-}T/T_c^*)$ for temperature close to the superconducting transition temperature T_c^* of the intergrain junction [7]. For the SNS-type proximity junctions, close to T_c^* the $I_c(T)$ dependence can be written in the form I_c=const $(1\text{-}T/T_c^*)^2$ [8]. To identify the character of weak links we tried to find the dependence of I_c on temperature for T close to the critical temperature T_c of a sample. The obtained dependence of I_c on $(1\text{-}T/T_c)$ were plotted on a logarithmic scale in order to determine the value of β in the equation I_c=const $(1\text{-}T/T_c)^\beta$ (Fig. 3). As can be seen, for D samples $I_c(T)$ corresponds to an SIS junction (β≈1). On the other hand, for S samples $I_c(T)$ agrees with an SNS type junction (β≈2) for any x value.

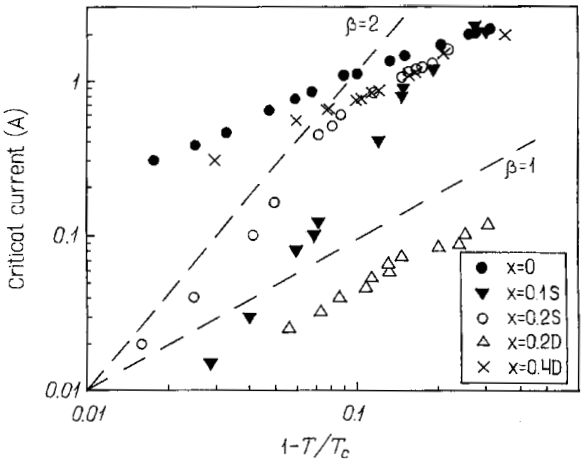

Fig. 3. Critical current versus $(1\text{-}T/T_c)$ plotted for D and S samples in a logarithmic scale to determine the value of b in the equation I_c=const $(1\text{-}T/T_c)^\beta$. β=1 and β=2 cases are shown by the dashed lines.

In this work a systematic statistical study of grain boundaries was made to correlate their distribution to the observed change in J_c when x varied from 0 to 0.4. So, 40–50 consecutive boundaries in each sample were characterized by bright field tilting imaging in TEM. The grain boundaries were distributed into 3 types. 'Clean' boundaries correspond to boundaries in which no intergranular phase was detected in TEM bright field. In contrast, 'dirty' boundaries exhibit an intergranular phase (thickness >2 nm). At last, 'thin-film-coated' boundaries display a thin phase with a thickness ≤2 nm. For clean boundaries, we paid attention on peculiarities such as dislocations, small facets or fine precipitates on them. One should take into account the fact that clean boundaries are favourable for transmitting the supercurrent only when the orientation crystallographic relationships between adjacent grains are suitable. Usually, no more than 50% of clean boundaries are considered as favourable. According to the data in [9], the percolation threshold is about 12%.

The histogram in Fig. 4 shows the statistical study results. In the D samples, the ratio of clean boundaries was found to remain between 27 and 45%. The proportion of clean boundaries decreased with x. The observed increase in J_c with x in D samples can be explained by the increase in the proportion of the faceted clean boundaries, which can act as pinning centres (Fig. 4). Ag doping resulted in a higher proportion of clean boundaries for x≥0.2, but there were only few faceted boundaries among them. For the composition with x=0.4, which exhibited 3 times increase in J_c, a peculiarity in the structure of clean boundaries was found, namely, about half of the clean boundaries contained

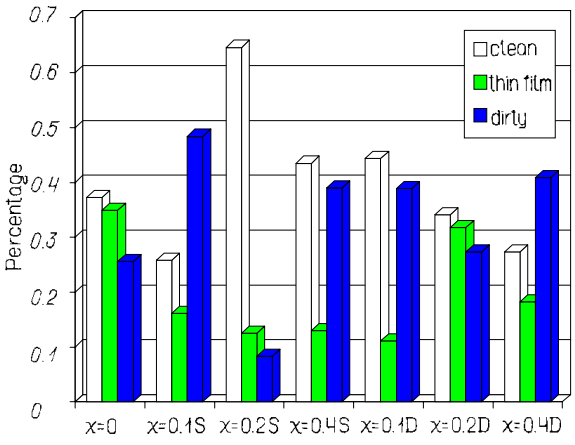

Fig. 4. Histogram showing the distribution of clean, thin-film-coated and dirty grain boundaries for a sample of the stoichiometric composition (x=0), D and S samples. The dashed lines show the fraction of faceted clean boundaries among all clean boundaries.

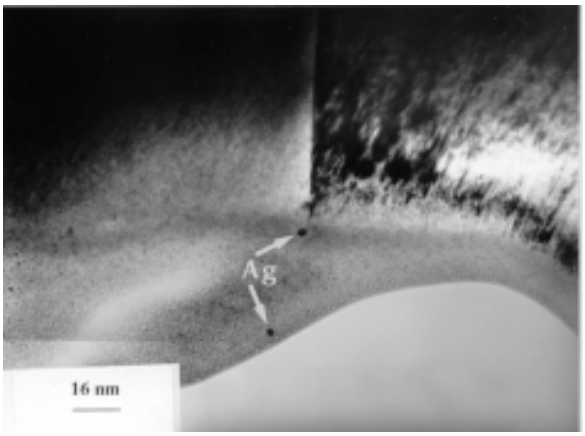

Fig. 5. Micrograph of a 'clean' boundary with Ag precipitates (shown by arrows) in TEM for an S sample (x=0.4).

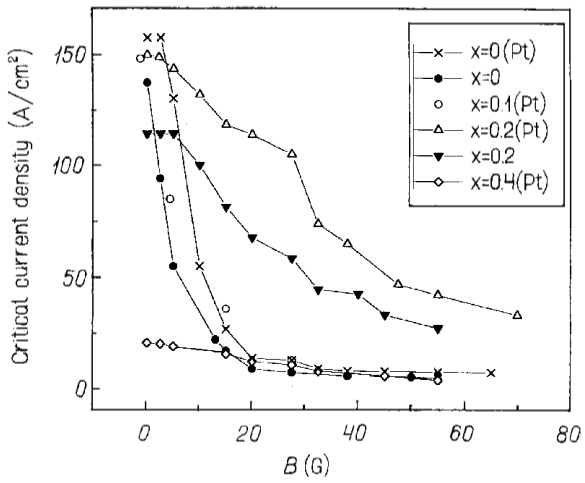

Fig. 6. Critical current density at 77 K versus applied magnetic field for $DyBa_2Cu_{3-x}O_y$/1wt.%Pt and $DyBa_2Cu_{3-x}O_y$ samples.

small precipitates of 2–5 nm in size on the boundary itself, or close to it (up to 5 nm). The average distance between these precipitates was about 30 nm. An example of such a 'clean' boundary with Ag precipitates is presented in Fig. 5. These small Ag precipitates can act as very efficient pinning centres resulting most likely in the 3-fold increase in J_c in this composition.

To detect possible Ag segregation at clean grain boundaries, EDX analysis in STEM with 1 nm probe was used. The detected concentration of Ag on some clean boundaries was twice higher than the obtained solubility limit of Ag in the grains (x=0.03). This increased Ag segregation on grain boundaries most probably leads to SNS behaviour of weak links in S samples as result of a percolation path of supercurrent through such 'clean' boundaries with an extremely narrow Ag segregation (≅1 nm) on them.

3.2 Cu-DEFICIENT DYSPROSIUM CERAMICS DOPED WITH 1 wt.% Pt

The next system studied was Cu-deficient dysprosium ceramics doped by Pt. Such a ceramic system was chosen due to the following reason. As we saw above, the deviation from stoichiometry leads to the formation of secondary phases in sintered ceramics. According to the literature data [10, 11], in melt-textured ceramics the addition of Pt can result in decrease in size of 211 secondary phase inclusions, improving thereby their pinning possibility and, then the critical current. In our work, for Cu-deficient dysprosium sitered ceramics doped with Pt, we tried again to identify microstructural elements, which can be responsible for the differences in superconducting properties.

In all compositions, Pt-doping resulted in the nucleation of intragranular secondary phases of submicron size, which contain Pt and were homogeneously distributed into 123 grains. In addition, in the non-stoichiometric composition, Pt was also located in intergranular $BaCuO_2$ secondary phases. Unlike the melt-textured 123 ceramics [10, 11], no influence of Pt on size and distribution of 211 secondary phase was found. Traces of Pt in the 123 grains were detected in all compositions doped by Pt. Distribution of Pt in the matrix was inhomogeneous. The maximum content of Pt in a grain was 0.06 molar content.

Fig. 6 displays the dependence of critical current density J_c on applied magnetic field. As seen, at zero-magnetic field doping with platinum practically does not change J_c in stoichiometric composition, but leads to its substantial increase for non-stoichiometric composition with x=0.2. The stoichiometric compositions exhibit a sharp drop of J_c values even in very low magnetic field. Non-stoichiometric compositions show a much smoother decrease in J_c with magnetic field. Doping with Pt strongly contributed to the so-called 'fish-tail' effect which means stabilization of J_c in magnetic field. For this composition this 'fish-tail' behaviour became more pronounced when the temperature was decreased (Fig. 7). So, the copper-deficient samples, especially the one doped with Pt seem to have better possibilities for pinning magnetic vortices in applied magnetic fields.

Similar to the system with Ag, for these ceramics with Pt we also tried to identify the character of the intergranular junction network from I_c versus temperature dependence (Fig. 8). Grain boundary network was found to behave predominantly as SIS junctions, even in Pt-doped samples so that Pt seems not to segregate in sufficient amount, at least, at grain boundaries. Within the accuracy of our EDX analysis we did not reveal higher concentration of Pt in boundaries compared with grains.

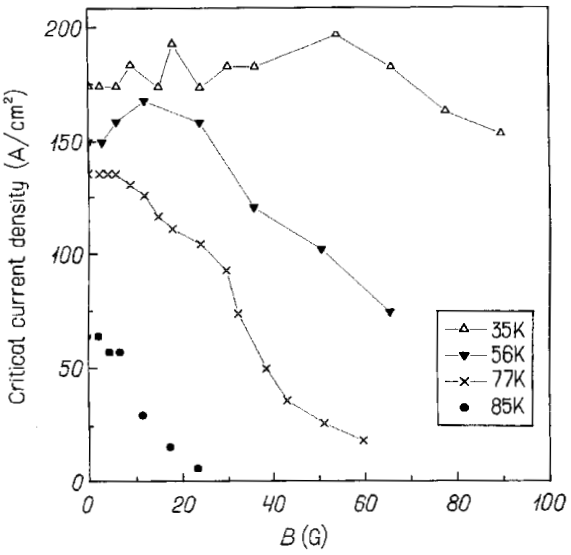

Fig. 7. Critical current density at 77 K versus applied magnetic field for $DyBa_2Cu_{2.8}O_y$/1wt.%Pt at different temperatures.

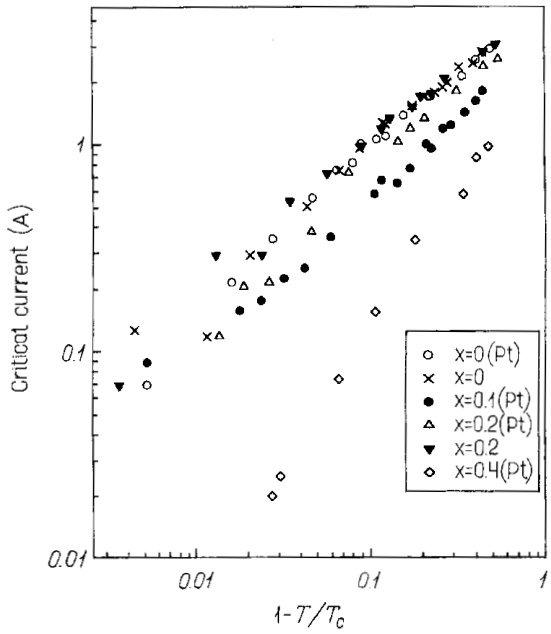

Fig. 8. Critical current versus $1\text{-}T/T_c$ plotted on logarithmic scale to determine the value β in the equation I_c=const $(1\text{-}T/T_c)^{\beta}$ for $DyBa_2Cu_{3-x}O_y$/1wt.%Pt and $DyBa_2Cu_{3-x}O_y$ samples.

The above superconducting properties were correlated with the microstructural features of the studied samples. In all compositions the 123 matrix exhibits well crystallized and well twinned grains, but with different twin density. It is known that twin boundaries in the 123 materials may act as flux pinning centres [12, 13]. In granular ceramics, where critical current is limited by weak links at grain boundaries, it is reasonable to consider twins near the boundaries. The higher the twin density the more efficient the pinning of vortices along the boundary. We compared the twin density in our compositions. As seen in the Table 2, in non-stoichiometric composition, the average spacing d between twins is twice smaller than in the stoichiometric one. In addition, in non-stoichiometric composition doped with Pt we locally observed very fine twins with d=20 nm, whereas in such composition only without Pt such a high density of twins was not found, at all. The presence of these highly dense twins can be caused by partial substitution of Cu by Pt in grains. A decrease of twin spacing due to Pt doping was observed in melt-textured 123 ceramics in [13, 14]. The higher density of twin boundaries in the vicinity of grain boundaries can improve the pinning properties under magnetic field. The highest local density of twins was observed in the composition, which exhibited the best 'fish-tail' effect in magnetic field.

We also performed comparative statistical study of grain boundaries, Table 3. It was found that in non-stoichiometric composition, unlike the stoichiometric one, grain boundaries are mostly clean or thin-film-coated. Doping with Pt resulted in a higher proportion of clean boundaries. Such statistical results can explain the sharp drop of I_c under very low magnetic fields (≤10 G) in $DyBa_2Cu_3O_y$/1wt.%Pt samples. As already noted above, no more than a half of clean boundaries can be considered as favourable [9]. So the supercurrent is likely to pass through a few thin-film-coated GBs resulting in the sharp drop in I_c in low magnetic fields. The non-stoichiometric compositions with x=0.2 have enough clean boundaries to provide the percolation path for supercurrent. A possibility for redistribution of the supercurrent through clean boundaries in a magnetic field and high dense twins locally observed can be reasons for better I_c behaviour in a magnetic field in non-stoichiometric composition doped with Pt.

CONCLUSION

(i) In all considered ceramic systems the critical current I_c is controlled by weak links at grain boundaries.

Table 2. The spacing between twins in DyBaCuO(Pt) samples.

	$DyBa_2Cu_3O_y$/1wt.%Pt	$DyBa_2Cu_{2.8}O_y$/1wt.%Pt	$DyBa_2Cu_{2.8}O_y$
Average twin spacing d	110 nm	50 nm (fine twins with d≈20 nm locally observed)	60 nm

Table 3. The distribution of clean, thin-film-coated and dirty grain boundaries in $DyBa_2Cu_{3-x}O_y$/1wt% Pt samples.

	$DyBa_2Cu_3O_y$/1wt% Pt	$DyBa_2Cu_{2.8}O_y$/1wt% Pt	$DyBa_2Cu_{2.8}O_y$
Clean	24 %	58 %	44 %
Thin-film	16 %	29 %	37 %
Dirty	56 %	5 %	15 %
Non-characterized	4 %	8 %	4 %

(ii) In Cu-deficient yttrium ceramics doped with Ag in amount equal the deficiency, Ag doping leads to change of type of the weak links from SIS to SNS-type. Such SNS behaviour is a result of percolation path of supercurrent through clean boundaries with extremely narrow (1nm) Ag-segregation on them. For x=0.4, decoration of clean boundaries by very fine Ag-precipitates (2–5 nm) is the most likely reason for 3 fold increase of critical current.

(iii) In non-stoichiometric composition with x=0.2, Pt-doping leads to pronounced increase in I_c and fish-tail effect in magnetic field. This may be associated with the substantial increase in proportion of clean boundaries and highly dense twins locally observed (due to Pt segregation in 123 grains). No noticeable segregation of Pt in grain boundaries was revealed.

REFERENCES

[1] S.E. Babcock and J.L. Vargas // *Annu. Rev. Mater. Sci*. **25** (1995) 193.

[2] R.S. Liu, W.N. Wang, C.T. Chang and P.T. Wu // *Japan. J. Appl. Phys.* **28** (1989) L2155.

[3] D.F. Lee, X. Chaud and K. Salama // *Physica C* **181** (1991) 81.

[4] J. Joo, J.P. Singh, R.B. Poeppel, A. K. Gangopadhyay and T.O. Mason // *J. Appl. Phys.* **71** (1992) 2351.

[5] C. Nguyen-van-Huong, E. Crampin, J.Y. Laval and A. Dubon // *Supercond. Sci. Technol.* **10** (1997) 85.

[6] R.L. Peterson and J.W. Ekin // *Physica C* **157** (1989) 325.

[7] J. Jung, I. Isaac and A.-K. Mohamed // *Phys. Rev. B* **48** (1993) 7526.

[8] P.G. DeGennes // *Rev. Mod. Phys.* **36** (1964) 225.

[9] V.K.S. Shante and S. Kirpatrick // *Adv. Phys.* **20** (1971) 325.

[10] M. Murakami, S. Gotoh, N. Koshizuka, S. Tanaka, T. Matsushita, S. Kanube and K. Kitazama // *Cryogenics* **30** (1990) 390.

[11] M. Murakami, H. Fujimoto, S. Gotoh, K. Yamagushi, N. Koshizuka and S. Tanaka // *Physica C* **185-189** (1991) 321.

[12] A.H. King and Y. Zhu // *Phil. Mag.* A **67** (1993) 1037.

[13] I. Monot, K. Verbist, M. Herview, P. Laffez, M.P. Dalamare, J. Wang, G. Desgardin and G.V. Tendeloo // *Physica C* **274** (1997) 253.

[14] M.P. Delamare, M. Hervieu, J. Wang, J. Provost, I. Monot, K. Verbist and G.V. Tendeloo // 1996 *Physica C* **262** (1996) 220.